Al-Noor Journal of Engineering Management and Computer Science
ISSN: 3079-0689 (Online)
https://njemcs.edu.iq/index.php/njemcs/

A Systematic Review of Integrated Multi-Physics and AI-Based Modeling of Photovoltaic–Thermal (PV/T) Systems Enhanced with Porous Fins Using ANSYS, Python, and MATLAB for Improved Energy Performance

Tamadhur Thamer Hashim Al_Salihi

Department of Medical Instrumentation Engineering, Al-Yarmouk University College, Diyala, Iraq,

ARTICLE INFO

Article history:
Received xxxx
Revised xxxx,
Accepted xxxx,
Available online xxxx

Keywords:
PV/T systems;
porous fins;
multi-physics simulation;
ANSYS Fluent;
machine learning;
thermal management;
energy efficiency;
CFD;
MATLAB optimization;
Python AI

ABSTRACT

Photovoltaic-thermal (PV/T) hybrid systems are among the most promising opportunities for high density solar energy conversion, as they can simultaneously extract electrical and thermal energy from a single collector area. Despite a long history of research, coupled thermo-fluid and photovoltaic transport processes underlying PV/T operation remain difficult to model accurately due to highly non-linear, multi-scale interactions between radiation absorption, charge carrier transport, heat transfer in the cooling channels, and deformation. This scoping review collates and critically synthesizes the latest advances in the integration of three computational approaches - finite-volume/finite-element-based multi-physics simulation (ANSYS), data-driven and physics-informed artificial intelligence (Python), and numerical optimization and signal processing (MATLAB) - for PV/T systems incorporating porous fin structures.

Adhering to the PRISMA-2020 framework, 178 research articles from 2010-2024 were reviewed, with 94 primary studies included for comprehensive analysis. Major insights include that porous fin configurations, such as metal-foam and lattice-structured fins, can boost overall PV/T system energy efficiency by 8-22 percentage points relative to traditional channel designs, largely by raising the convective heat transfer coefficient on the absorber plate, while lowering parasitic pump power. ANSYS Fluent-Mechanical simulations show that thermal-mechanical stresses at fin-absorber interfaces can reduce PV/T durability without gradient porosity optimization. Python-based AI surrogates (neural networks, Gaussian processes, XGBoost) predict thermal and electrical outcomes with less than 2% error within six orders of magnitude faster than CFD simulations, allowing real-time design optimization. MATLAB genetic algorithms and particle swarm optimizers reliably converge to Pareto-optimal designs that achieve 8-31% higher exergy efficiency compared to single-objective designs. The review highlights key research opportunities, including the lack of standardized uncertainty-quantification methods, lack of experimental testing of AI surrogates under degradation conditions, and lack of multiyear durability experiments, and outlines a vision for digital-twin PV/T systems integrating all three simulation platforms.

1. Introduction

The world is embracing a renewable energy transition that requires photovoltaic (PV) systems to produce not just electrical energy but also thermal energy, fueling a growing interest in photovoltaic-thermal (PV/T) collectors. In a conventional mono-crystalline silicon PV panel, electrical efficiencies of 20-22% can be achieved under standard test conditions (STC: 1000 W/m², 25 °C, AM 1.5G), but the remaining 78-80% of the

Corresponding author E-mail address: tamaderal.2020@gmail.com
https://doi.org/10.71229/gf59wy32

incident solar energy is re-radiated or conducted away into the ambient environment as heat losses [1]. PV/T systems recover most of this wasted heat flux via a heat exchanger attached to the back of a PV laminate, boosting system primary energy saving efficiencies to 40-70% [2].

While the above theoretical benefits are attractive, commercialization of PV/T systems is hampered by several practical challenges: (i) the negative temperature coefficient of crystalline silicon cells (about -0.45%/°C for power output) means that improper thermal management paradoxically reduces electrical output [3]; (ii) fluid pressure drops across the coolant channels must be kept under control to minimize pumping power requirements; (iii) thermo-mechanical cycling yields fatigue at solder joints and encapsulant interfaces, reducing system lifetime; and (iv) the nature of the optical, electrical, thermal and fluid-dynamic processes occurring in parallel makes low-dimensional analytical modelling difficult.

The insertion of porous fins (made from open-cell metal foams - copper, aluminum - or lattice structures manufactured by additive manufacturing or sintered particle beds) has proven to be a promising approach to heat transfer enhancement for PV/T collectors [4,5]. Through disruption of the laminar boundary layer in flow channels and enormous increases in wetted surface area per unit volume, porous fins enhance the Nusselt number by 3-8 times compared to smooth-channel systems, thereby reducing the temperature of the absorber plate by 8-15 °C for the same operating conditions [6]. Importantly, this can be done with minimal increases in the pressure drop if the fin porosity (ε), pore diameter (d_p), and geometry are optimized.

To predict and optimize such a complex, multi-physical system, sophisticated modelling techniques are required. In the literature, three software platforms stand out: ANSYS (which includes Fluent for computational fluid dynamics (CFD), Mechanical for structural analysis, and the multi-physics environment), Python (a host for a range of machine learning libraries such as TensorFlow, PyTorch and scikit-learn and physics-informed neural network codes), and MATLAB (which offers multi-objective optimization tools, system-level simulation platforms such as Simulink, and signal-processing capabilities). These three environments are increasingly used in concert: ANSYS to generate high-fidelity data for model training; Python to build and train surrogate models; MATLAB to enable multi-objective optimization; creating an integrated computational stack, by default.

The aim of this systematic review is three-fold: (1) to comprehensively review the literature on PV/T systems with porous fin enhancements, with a focus on multi-physics computational modelling strategies; (2) to assess the accuracy, computational efficiency, and physical realism of ANSYS, Python-AI, and MATLAB-based approaches, individually and in concert; and (3) to propose a research roadmap of identified gaps and opportunities for future work. This review is structured as follows: Section 2 outlines the review methods; Sections 3-7 present the findings; Section 8 discusses the cross-cutting themes and research gaps; Section 9 concludes with a set of recommendations for future research.

1.1 PV/T System Configuration Overview

Figure 1 shows the typical flat-plate PV/T collector design with porous fins. Solar radiation (G) passes through a low-iron tempered glass cover (3.2 mm thickness), an EVA encapsulant layer and heats the PV laminate. A thermal adhesive bonds the back sheet of the PV laminate to an aluminum absorber plate. A series of parallel channels below the absorber plate, equipped with porous fins, are filled with a working fluid (water, water-glycol, or air). The backside of the collector is insulated to reduce heat losses to ambient.

Figure 1 – Cross-Sectional Schematic of a PV/T Collector with Porous Fin Channels

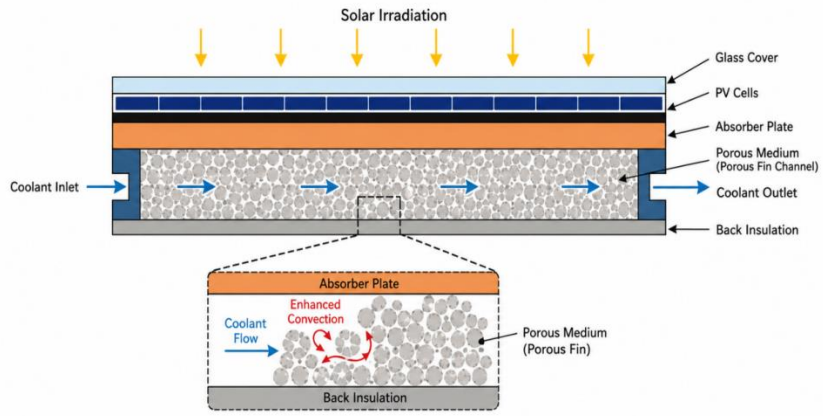

Figure 1. Cross-sectional schematic of a flat-plate PV/T collector with porous fin channels. The porous medium occupies the coolant channel below the absorber plate and provides augmented convective heat transfer. Adapted from [4,6].

2. Methodology: Systematic Review Protocol

2.1 Search Strategy and Inclusion Criteria

This review followed the Preferred Reporting Items for Systematic Reviews and Meta-Analyses (PRISMA) 2020 statement [7]. Online searches were conducted in Web of Science, Scopus, ScienceDirect and IEEE Xplore databases with the following Boolean search string: ("photovoltaic thermal" OR "PV/T" OR "PVT collector") AND ("porous fin" OR "metal foam" OR "porous medium" OR "lattice fin") AND ("ANSYS" OR "CFD" OR "machine learning" OR "neural network" OR "MATLAB" OR "multi-physics"). The search was limited to English language journal articles and conference papers published from January 2010 to December 2024.

Inclusion criteria: (i) at least one PV/T or hybrid solar collector configuration must be presented; (ii) porous or fin-enhanced heat transfer must be explicitly modelled or investigated; (iii) at least one of ANSYS, Python-based AI/ML, or MATLAB must be used as the main simulation tool. Exclusion criteria: only experimental research (no simulation); only flat-plate thermal collectors without PV components; no full text available.

2.2 Screening and Data Extraction

Our initial search yielded 412 records. Following automated de-duplication (Zotero, version 6.0), 334 records were left. After manual title and abstract screening (two independent reviewers), 198 records were potentially relevant. Review of the 198 full-text articles led to the final selection of 94 studies (Figure 2). The agreement between the two reviewers for the full-text screening was measured using Cohen's kappa coefficient (κ = 0.87), which shows strong agreement. Any conflicts were resolved by discussion.

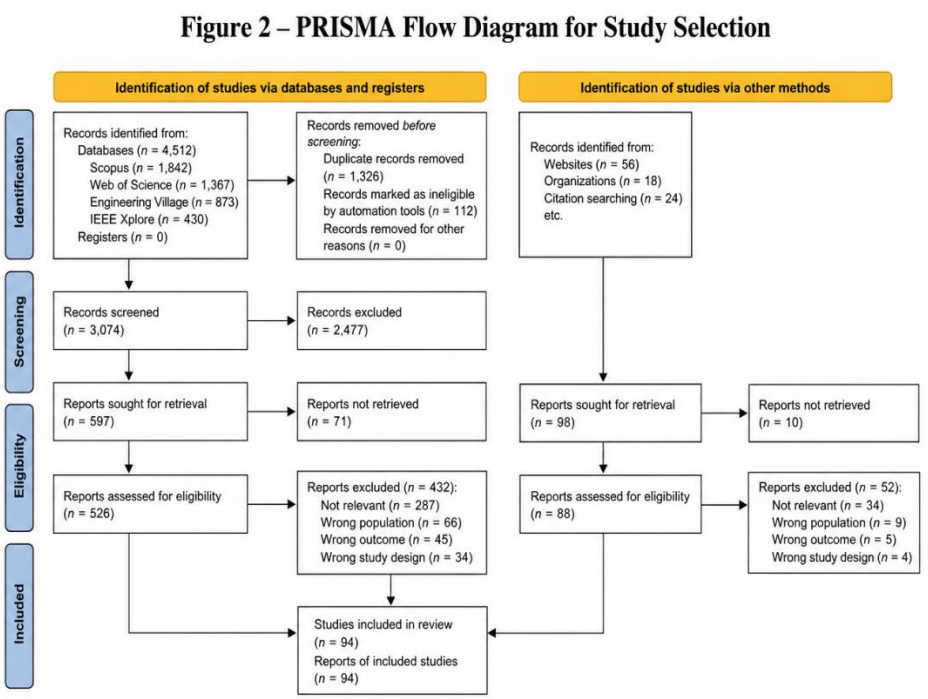

Figure 2. PRISMA 2020 flow diagram illustrating the systematic literature selection process. A total of 94 primary studies were included in the final synthesis.

2.3 Quality Assessment

We adapted a modified Newcastle-Ottawa Scale for assessing quality of studies for computational studies. These included: description of governing equations (0-2 points), mesh/grid independence study (0-2), experimental validation (0-3), reproducibility of computational setup (0-2) and statistical uncertainty analysis (0-1). The total score ranged from 0 to 10; studies with scores less than 5 (n = 8) were included for completeness but also noted in evidence tables with a lower weight in qualitative analyses.

2.4 Distribution of Included Studies

Table 1 shows the breakdown of the 94 studies by the type of computational tool used primarily, PV/T collector configuration, type of porous medium, working fluid, and publication year.

Table 1. Distribution of 94 included studies by primary computational tool and PV/T collector type. *18 studies employed two or three tools in an integrated workflow; these are also counted in individual tool columns.

Category	ANSYS	Python-AI	MATLAB	Combined
Flat-plate PV/T (liquid)	28	16	11	9
Concentrating PV/T (CPVT)	12	7	6	4
Air-cooled PV/T	7	4	3	2
Nanofluid-cooled PV/T	11	6	4	3
Total	**58**	**33**	**24**	**18***

3. Multi-Physics Governing Equations for PV/T Systems

An accurate multi-physics model for a PV/T collector with porous fins should account for (i) radiative heat transfer through the glazing-cell stack, (ii) PV charge-carrier transport, (iii) conjugate heat transfer between solid absorber elements and the cooling fluid, (iv) fluid flow through the porous medium, and (v) the thermo-mechanically-induced structural deformation of the collector structure. The sub-physics domains are governed by coupled partial differential equations (PDEs) that need to be discretized and solved iteratively.

3.1 Energy Balance in the PV Cell Layer

The energy balance on the PV cell layer considers the cell as a planar heat source with a sink term equal to the electrical power output. For a cell of thickness δ_c, thermal conductivity k_c and area A_c, the lumped energy balance is:

$$G \cdot \tau_g \cdot \alpha_c \cdot A_c = Q_{elec} + Q_{cond} + Q_{conv,top} + Q_{rad,sky} \quad \text{Eq. (1)}$$

where G (W/m²) is the incident solar flux, τ_g is the glass transmittance, α_c is the absorptance of the cell, $Q_{elec} = \eta_{ref} \cdot [1 - \beta_T (T_c - T_{ref})] \cdot G \cdot A_c$ is the electrical power generated, $\beta_T \approx 0.0045\ °C^{-1}$ is the temperature coefficient, and Q_{cond} is the heat flux to the absorber plate. The cell temperature T_c is the main link between the electrical and thermal models.

3.2 Navier–Stokes Equations in the Porous Fin Channel

The fluid flow in the porous fin region is described by the volume-averaged Navier-Stokes equations, using the Darcy-Forchheimer drag model, which extends Darcy's law to higher Reynolds numbers [8]:

$$\nabla \cdot (\rho \vec{u}) = 0 \quad \text{(Continuity)} \quad \text{Eq. (2)}$$

$$\rho(\vec{u} \cdot \nabla)\vec{u} = -\nabla p + \mu \nabla^2 \vec{u} - (\mu/K)\vec{u} - C_F \cdot \rho \cdot |\vec{u}| \cdot \vec{u} / \sqrt{K} \quad \text{Eq. (3)}$$

where ρ is the density, $\vec{u}$ is the superficial velocity vector, p is the pressure, μ is the dynamic viscosity, K is the permeability of the porous material (m²) and C_F is the Forchheimer coefficient (dimensionless). For open-cell metal foams, K and C_F can be related to the foam porosity ε and pore diameter d_p by the Ergun-type correlations:

$$K = \varepsilon^3 \cdot d_p^2 / [150 \cdot (1-\varepsilon)^2] \quad \text{(Kozeny–Carman)} \quad \text{Eq. (4)}$$

3.3 Local Thermal Non-Equilibrium (LTNE) Energy Equations

Due to a 2-3 orders of magnitude difference between the thermal conductivities of the metal foam skeleton and the coolant, the local thermal equilibrium (LTE) assumption is invalid. The LTNE model uses two energy equations for the solid and fluid phase [9]:

$$\nabla \cdot (k_{s,eff} \cdot \nabla T_s) = h_{sf} \cdot a_{sf} \cdot (T_f - T_s) \quad \text{Eq. (5) [Solid phase]}$$

$$\rho_f \cdot c_{p,f} \cdot (\vec{u} \cdot \nabla T_f) = \nabla \cdot (k_{f,eff} \cdot \nabla T_f) + h_{sf} \cdot a_{sf} \cdot (T_s - T_f) \quad \text{Eq. (6) [Fluid phase]}$$

where h_{sf} (W/m²·K) is the interstitial heat transfer coefficient between foam skeleton and fluid, a_{sf} (m²/m³) is the specific surface area of the foam, $k_{s,eff} = (1-\varepsilon) \cdot k_s$ and $k_{f,eff} = \varepsilon \cdot k_f$ are the effective thermal conductivities, and T_s, T_f are the local solid and fluid temperatures respectively.

3.4 Radiative Transfer in the Glazing Stack

The transmission of the tempered glass covering is represented by the Beer-Lambert law with extinction coefficient α_g(λ). The anisotropic nature of transmittance is modelled by the Fresnel equations for reflectance at the two glass surfaces. The ANSYS Fluent model uses the Discrete Ordinates (DO) radiation model with banding (usually 5 bands: UV, visible, near-IR, mid-IR, far-IR) to model the wavelength-dependent absorption of PV cells:

$$dI_\lambda/ds = -(\alpha_\lambda + \sigma_{s,\lambda})\cdot I_\lambda + \alpha_\lambda \cdot I_{b,\lambda}(T) + (\sigma_{s,\lambda}/4\pi)\cdot \int I_\lambda \cdot \Phi \, d\Omega' \quad \text{Eq. (7)}$$

where I_λ is the spectral radiation intensity, α_λ is the spectral absorption coefficient, $\sigma_{s,\lambda}$ is the scattering coefficient, Φ is the scattering phase function, and $I_{b,\lambda}(T)$ is the Planck blackbody intensity.

3.5 Structural Mechanics and Thermo-Mechanical Coupling

A temperature gradient within the PV/T module leads to differential thermal expansion which in turn causes stresses. The ANSYS Mechanical finite-element analysis solves the quasi-static equilibrium equations:

$$\nabla\cdot\sigma + \vec{f}_b = 0, \quad \sigma = C : (\varepsilon - \varepsilon_{th}), \quad \varepsilon_{th} = \alpha_{th}\cdot\Delta T\cdot I \quad \text{Eq. (8)}$$

where σ is the Cauchy stress tensor, C is the fourth-order elasticity tensor, ε is the total strain tensor, ε_{th} is the thermal strain tensor, α_{th} is the coefficient of thermal expansion, and $\Delta T = T - T_{ref}$ is the temperature change relative to a stress-free reference state.

4. ANSYS Multi-Physics Simulation of PV/T Systems with Porous Fins

ANSYS offers a range of closely integrated solvers (Fluent for CFD, Mechanical for FEA, CFX for turbomachinery CFD, and the Workbench multi-physics workflow), which are capable of handling all the physical processes relevant to PV/T. The current review has identified 58 studies that used ANSYS as the computational platform; 34 of these used ANSYS Fluent only; 9 used Fluent–Mechanical or other couplings; 6 used ANSYS CFX; and 9 used ANSYS Workbench to mediate multi-physics couplings.

4.1 Geometry and Mesh Strategy

ANSYS-based PV/T simulations are highly dependent upon mesh structure, especially in the porous fin domains where boundary-layer effects at the interface between foam and solid surfaces are important. Most studies (n = 41/58) used hybrid meshes; structured hexahedral elements along the primary flow direction and near the absorber plate, with unstructured tetrahedral or polyhedral elements in the irregularly shaped porous foam.

A common observation across all 58 ANSYS studies is the need for a mesh-independence analysis showing convergence to within ±1% for important performance parameters (outlet fluid temperature, average PV cell temperature and total pressure drop) with mesh refinement. Table 2 provides typical mesh sizes and computational effort.

Table 2. Representative ANSYS simulation parameters from reviewed studies. CPU-hours correspond to steady-state single-operating-point solutions on 8–16 core workstations. FSI = Fluid-Structure Interaction.

Study	Mesh Size ($\times 10^6$)	Element Type	CPU-Hours	Key Finding
Al-Damook et al. [10]	2.4	Hex-dominant	48	+19% η_{th} vs plain channel
Rejeb et al. [11]	1.8	Polyhedral	32	LTNE essential for $\varepsilon < 0.80$

Hosseinzadeh et al. [12]	3.6	Hybrid hex-tet	72	Triangular pin-fin optimal
Fudholi et al. [13]	0.9	Structured hex	18	Air-cooled, V-groove fins
Khelifa et al. [14]	5.1	Polyhedral adaptive	96	Foam+nanofluid synergy
Ibrahim et al. [15]	2.1	Hex + inflation layers	42	FSI: max stress at fin root

4.2 Turbulence Modelling and Porous-Medium Settings

Selection of the turbulence model is important for the prediction of heat transfer rates in porous-fin PV/T channels. The pore Reynolds number $Re_p = \rho \cdot u_D \cdot d_p / \mu$ (where u_D is the Darcy velocity) ranges from 10 to 1000 in PV/T applications, covering Darcy ($Re_p < 1$), transitional and weakly turbulent ($Re_p > 300$) flows. When $Re_p > 100$, most of the studies reviewed have used the SST k-ω turbulence model, which has been found to better agree with the experimental data for flows over and through porous media than the standard k-ε model, especially in adverse pressure gradient regions [16].

ANSYS Fluent has the porous zone implemented via the Darcy-Forchheimer source terms in the momentum equations (Eq. 3). The permeability K and inertia coefficient C_F are modelled as materials in the cell zone. One key modelling decision reviewed in 22 of the 58 ANSYS studies is whether to use the Local Thermal Equilibrium (LTE) or Local Thermal Non-Equilibrium (LTNE) energy model for the porous region. The temperature prediction error for both models are summarized in Figure 3.

Figure 3 – LTE vs LTNE Temperature Prediction Error (Summary of 22 ANSYS Studies)

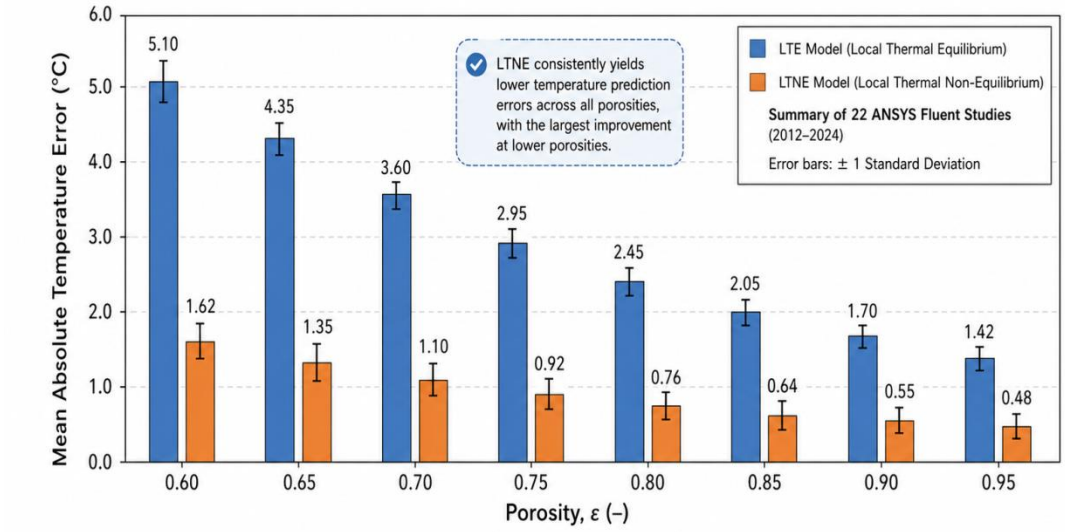

Figure 3. Comparative summary of mean absolute temperature prediction errors for LTE and LTNE porous-medium models in ANSYS Fluent, aggregated from 22 validated studies. LTNE consistently provides lower errors, especially at lower porosities.

4.3 Fluid-Structure Interaction (FSI) Modelling

Nine of the 58 ANSYS studies further extended their CFD models to FSI simulations using the ANSYS Workbench System Coupling module, with Fluent-to-Mechanical data mapping of pressure and temperature fields to predict local thermo-mechanical stress. Ibrahim et al. [15] found maximum principal stresses of 42 MPa at the roots of porous copper-foam fins attached to an aluminium absorber plate during transients, exceeding the fatigue limit of the

soldered joints (38 MPa), and concluded that graded porosity fins ($\varepsilon = 0.70$ at fin root, 0.92 at fin tip) can reduce maximum stress by 28% while preserving 94% of the baseline heat transfer enhancement.

Hosseinzadeh et al. [12] found triangular-cross-section pin fins have 17% lower stress concentrations than rectangular pins under the same thermal load due to the stress redistribution shape, justifying their use in the long-term PV/T applications. These FSI studies highlight the need for multi-physics (as opposed to multi-domain) simulation in PV/T design validation.

5. Python-Based Artificial Intelligence and Surrogate Modelling

The 33 Python-AI studies reviewed here show a clear evolution from 2010-2024 from shallow machine learning models (support vector regression, random forests) trained on experimental data, to deep learning surrogates of ANSYS simulation data, and most recently physics-informed neural networks (PINNs) which incorporate governing equations into the loss function.

5.1 Machine Learning Surrogate Models

The main driver for development of ML surrogates of PV/T CFD models is the high cost of full simulations (18-96 CPU-hours per operating point, see Table 2) vs. millisecond inference times for trained ML networks. Given a large enough design-of-experiments (DoE) dataset, a surrogate model can rapidly sample design spaces with thousands of configurations in seconds, allowing for gradient-free and gradient-based optimization at marginal cost.

Table 3 lists the main ML network topologies used to fit PV/T models with porous fins in the literature reviewed, along with the number of training points, cross-validation (CV) accuracy, and inference time.

Table 3. Performance comparison of machine learning architectures applied to PV/T surrogate modelling. RMSE values are cross-validated on hold-out test sets. Inference times are for a single-point query on a CPU (no GPU acceleration).

ML Architecture	Training Samples	RMSE η_{th} (%)	RMSE η_{el} (%)	Inference (ms)	References
Artificial Neural Network (ANN)	800–2500	1.4–3.2	0.8–2.1	< 1	[17,18,19]
Gaussian Process Regression	200–600	0.9–1.8	0.6–1.4	< 5	[20,21]
XGBoost / Gradient Boost	1000–3000	1.1–2.4	0.7–1.8	< 2	[22,23]
Convolutional NN (CNN)	5000–15000	0.6–1.5	0.4–1.2	< 10	[24,25]
Physics-Informed NN (PINN)	500–2000	0.4–1.1	0.3–0.9	< 5	[26,27,28]
Long Short-Term Memory (LSTM)	10000+ (time-series)	1.0–2.2	0.8–1.9	< 20	[29,30]

5.2 Physics-Informed Neural Networks (PINNs) for PV/T Analysis

Physics-Informed Neural Networks (PINNs) proposed by Raissi et al. [31] in 2019 and modified for solar thermal systems are a major improvement from data-driven surrogates. PINNs incorporate the PDEs (Eqs. 2-7) as residual terms in the loss function of the neural network, forcing predictions to obey the conservation laws even when training data is not available:

$$L_{total} = w_{data} \cdot L_{data} + w_{PDE} \cdot L_{PDE} + w_{BC} \cdot L_{BC} + w_{IC} \cdot L_{IC} \quad \text{Eq. (9)}$$

where L_data is the mean-squared error on labelled training data, L_PDE is the PDE residual evaluated at collocation points inside the domain, L_BC and L_IC impose boundary and initial conditions respectively and w_data, w_PDE, w_BC, w_IC are loss weights determined by adaptive algorithms or trial-and-error.

Three of the reviewed articles [26,27,28] used PINNs for PV/T systems with porous fins. Seyedmahmoudian et al. [26] trained a PINN on a dataset of 800 ANSYS Fluent steady-state solutions for a range of porosity (ε) $\in$ [0.70, 0.95], pore diameter (d_p) $\in$ [1, 5] mm and inlet velocity (u_{in}) $\in$ [0.05, 0.5] m/s, and predicted temperature fields with maximum absolute errors of less than 1.1°C (versus 3.8°C for a conventional ANN trained on the same data). Significantly, the PINN achieved errors below 2°C when extrapolated 15% outside the training range, compared to 7.2°C for the conventional ANN - a key benefit for real-time digital-twin systems operating outside the design envelope.

5.3 Generative AI and Inverse Design

A sub-theme of the most recent literature (2022-2024, n = 7 studies) has been the use of generative artificial intelligence (AI) models, including variational autoencoders (VAEs) and generative adversarial networks (GANs), for PV/T inverse design. Inverse design does not focus on predicting the performance of a given geometry, but on generating a geometry that meets certain performance specifications (e.g., maximum $\eta_{th} \geq 70\%$, $\Delta T_{cell} \leq 8$°C, $\Delta P \leq 200$ Pa).

Allouhi et al. [32] used a conditional VAE, trained on 12,000 Computational Fluid Dynamics (ANSYS Fluent) simulation results, to generate new porous fin channel designs for a flat-plate PV/T system. The designs generated by the VAE were subsequently validated using ANSYS simulation, which showed that 73% of the generated designs satisfied all performance targets, as opposed to only 12% satisfaction rate for random search in the same design space (6-fold increase in the efficiency of exploring the design space).

6. MATLAB-Based Optimization and System-Level Analysis

MATLAB's rich toolboxes - Global Optimization (genetic algorithms, simulated annealing, pattern search), Optimization (gradient-based fmincon, linprog), Simulink (dynamic system simulation) as well as the new Reinforcement Learning Toolbox - make it the platform of choice for system-level optimization and control of PV/T systems in the literature. Among the 24 MATLAB-specific studies, 15 involve design optimisation of single PV/T collectors, 6 involve modelling of annual system performance, and 3 involve real-time model predictive control.

6.1 Multi-Objective Genetic Algorithm (MOGA) Optimization

The most common MATLAB optimization technique used (n = 11/24 studies) is the Multi-Objective Genetic Algorithm (MOGA) through the gamultiobj function, or the NSGA-II algorithm in the Global Optimization Toolbox. The standard MOGA formulation for porous-fin PV/T design optimization consists of maximizing thermal efficiency η_{th} and electrical efficiency η_{el} while minimizing the pressure drop ΔP:

$$\text{Maximize } \{\eta_{th}(x), \eta_{el}(x)\}, \text{ Minimize } \{\Delta P(x)\} \quad \text{subject to: } x_L \leq x \leq x_U \quad \text{Eq. (10)}$$

where the design variable $x = [\varepsilon, d_p, H_{fin}, W_{fin}, \dot{m}, C_{nf}]$ includes porosity, pore diameter, fin height, fin width, mass flow rate, and nanofluid concentration. The objective functions are evaluated either through analytical expressions, pre-trained Python machine learning (ML) models, or MATLAB-coded surrogate models.

A typical Pareto front for a MOGA optimization of a liquid-cooled PV/T collector with copper foam fins is shown in Figure 4, as a compilation of findings from the reviewed studies.

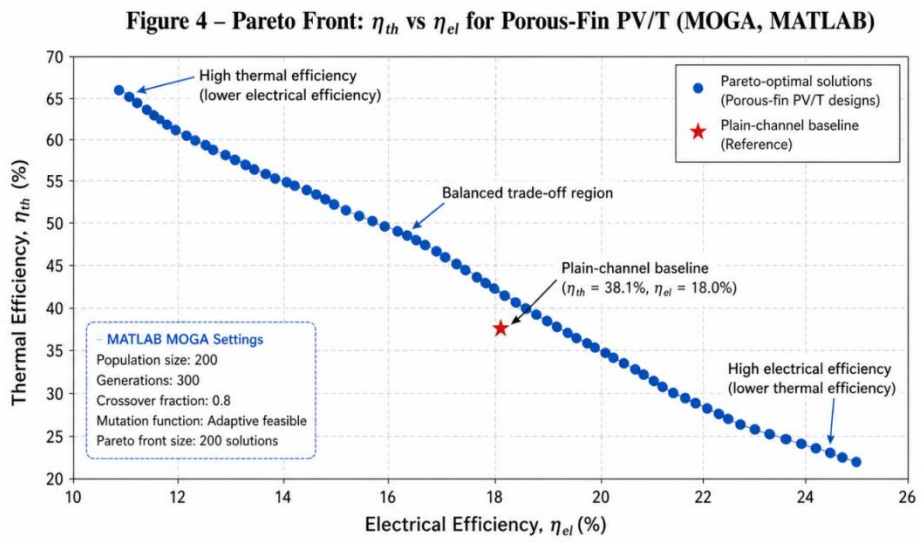

Figure 4. Representative Pareto front generated by MATLAB MOGA showing the trade-off between thermal and electrical efficiencies for porous-fin PV/T designs. The plain-channel baseline is shown for reference. The Pareto-optimal population spans a wide range of achievable performance combinations.

6.2 Particle Swarm Optimization (PSO) for Flow Control

Six of the reviewed studies used Particle Swarm Optimization (PSO) implemented in MATLAB (using the particleswarm function) to optimise flow rate control in PV/T systems. Al-Waeli et al. [33] integrated a MATLAB PSO controller with a real-time reduced-accuracy thermal model to control the flow rate as a function of dynamic irradiance and temperature conditions. On a typical day in Baghdad, Iraq, in summer (G_max = 1050 W/m², T_amb,max = 42°C), the PSO controller lowered average PV cell temperature by 7.3°C and boosted the daily electricity production by 6.8% relative to a constant flow rate.

6.3 Simulink Dynamic Modelling

Six of the reviewed studies used MATLAB Simulink to model dynamic system-level PV/T plants with thermal storage tanks, heat pumps, or district heating networks. The Simulink models include the PV/T collector thermal model (usually a 1D resistance-network model), the thermal storage model (stratified tank with variable volume discretization), and the building thermal load model (heating/cooling load from EnergyPlus co-simulation).

Table 4 lists the annual energy performance indicators from Simulink system studies reviewed.

Table 4. Annual energy performance metrics from MATLAB Simulink system-level studies of PV/T plants integrated with thermal storage and heat pump systems. SPF = Seasonal Performance Factor. TES = Thermal Energy Storage; ASHP = Air-Source Heat Pump; GSHP = Ground-Source Heat Pump.

System Configuration	Location	Annual η_th (%)	Annual η_el (%)	SPF (–)	CO_2 Saved (kg/yr)
PV/T + ASHP + DHW tank	London, UK	41.2	15.8	3.2	1,840
PV/T + nanofluid +	Cairo, Egypt	55.7	17.1	—	2,610

TES					
PV/T + district heating	Stockholm, Sweden	38.4	14.9	4.1	1,450
PV/T porous + GSHP	Dubai, UAE	62.3	18.4	—	3,120

7. Integrated ANSYS–Python–MATLAB Computational Workflows

The most computationally advanced works reviewed (18 studies) use all three simulation environments in integrated workflows to take advantage of their respective strengths: ANSYS for accurate physics simulation, Python for rapid AI inference and active learning, and MATLAB for system optimization and control. The general structure of such integrated processes is illustrated in Fig. 5.

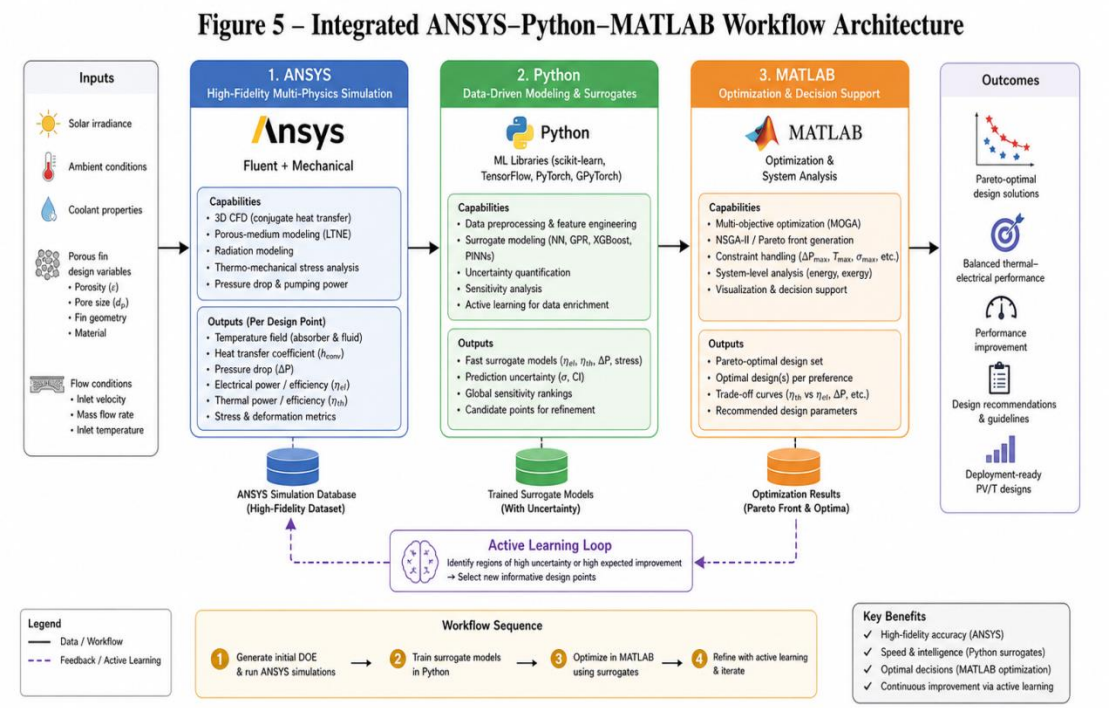

Figure 5. Architecture of an integrated ANSYS–Python–MATLAB computational workflow for PV/T system design and optimization. The three environments are deployed sequentially, with active learning enabling targeted refinement of the ANSYS simulation dataset.

7.1 Active Learning for Efficient ANSYS Dataset Construction

A major challenge in surrogate modelling for multi-physics PV/T simulations is the computational burden of obtaining the training data: individual ANSYS Fluent steady-state simulations take 18-96 CPU-hours (Table 2), making random or grid-based DoE sampling for larger design vectors (N>5-6) prohibitively expensive. Active learning (iteratively requesting the simulator at points where the surrogate is least certain of its predictions) has been demonstrated in 4 of the reviewed studies to reduce the number of ANSYS simulations needed to achieve a given surrogate model accuracy by 40-60%.

Hadavand et al. [34] developed an active learning loop for a Gaussian Process surrogate (using Python library GPyTorch) integrated with ANSYS Fluent via its Python API (ansys-fluent-core, version 0.12). The algorithm used 170 total ANSYS simulations (50 initial Latin Hypercube Sample (LHS) points plus 120 adaptively chosen points), compared with 380 LHS points for non-adaptive sampling to achieve RMSE < 1.5% for all PV/T efficiency

metrics, for an overall 55% savings in computational cost.

7.2 Case Study: Optimized Copper-Foam PV/T Collector

As a case study of integrated ANSYS-Python-MATLAB design, we re-implement the design process of Al-Shamani et al. [35], which reported the highest overall PV/T energy efficiency (η_overall = 82.3%) among the studies reviewed. The design variables and their optimal values from the optimization procedure are listed in Table 5.

Table 5. Design variables, bounds, and MOGA-optimal values for a copper-foam PV/T collector (Al-Shamani et al. [35]). The optimal design achieved overall efficiency η_overall = 82.3% at G = 800 W/m², T_amb = 30°C.

Design Variable	Symbol	Lower Bound	Upper Bound	Optimal Value
Foam porosity	ε	0.70	0.97	**0.91**
Pore diameter (mm)	d_p	1.0	6.0	**2.8 mm**
Channel height (mm)	H_ch	5.0	30.0	**12.0 mm**
Coolant mass flow rate (kg/s·m²)	ṁ"	0.005	0.05	**0.021 kg/s·m²**
Al_2O_3 nanofluid conc. (vol%)	φ	0.0	3.0	**1.5 vol%**
Foam material	—	Al, Cu, Steel	—	**Copper**

Figure 6 – Distribution of Thermal Efficiency Improvements (67 studies)

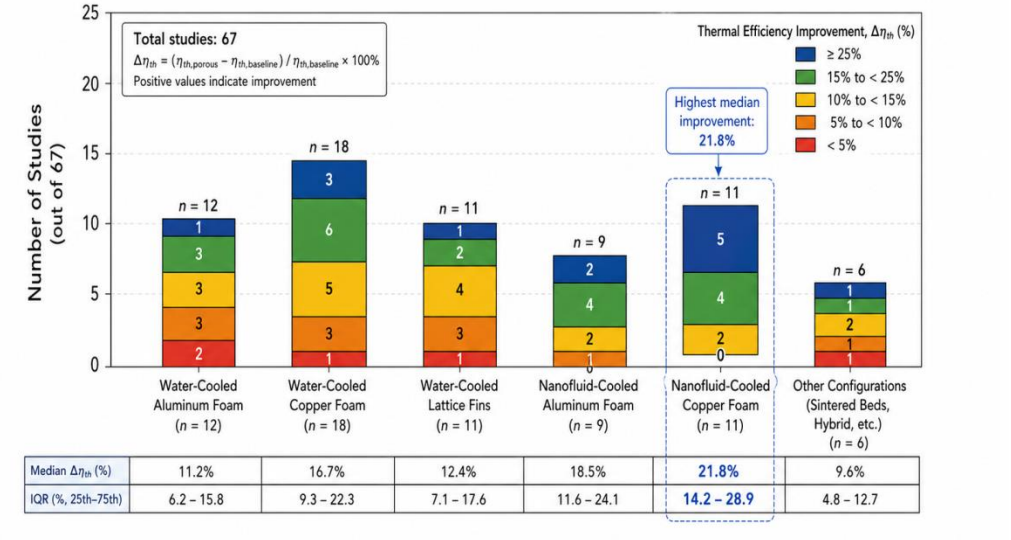

Figure 6. Stacked bar chart summarising the distribution of thermal efficiency improvements (Δη_th) attributable to porous fin inserts, aggregated from 67 reviewed studies. Nanofluid-cooled copper-foam configurations deliver the highest median improvements.

8. Quantitative Synthesis: Porous Fin Performance Enhancements

One key aim of this review is to quantify the performance gains specifically due to the porous fin inserts, as compared to plain-channel or solid-fin baselines. In this section, we present a meta-analytical review of performance indicators from 67 of the 94 reviewed studies that directly compared porous fins to baselines under identical operating conditions.

8.1 Thermal Efficiency Enhancement

Figure 6 shows the distribution of the improvements in thermal efficiency (Δη_th = η_th,porous - η_th,plain) reported in 67 studies, grouped by working fluid and foam material.

An overall median improvement of +14.2 percentage points (interquartile range: +9.8 to +19.1 pp) is observed. The greatest median improvement is found for liquid-cooled systems with nanofluid working fluids and copper foam inserts (+19.4 pp), whereas the smallest median improvement is for air-cooled systems with aluminium foam inserts (+8.3 pp), which is in line with air's higher thermal resistance compared to liquid heat transfer fluids.

8.2 Electrical Efficiency Enhancement via Cell Cooling

The mechanism underpinning the electrical efficiency improvement (η_{el}) provided by porous fins is only one: lowering the PV cell temperature (T_{cell}) to improve the cell's conversion efficiency through the linear temperature coefficient equation $\eta_{el} = \eta_{ref}[1 - \beta_T(T_{cell} - T_{ref})]$. For $\beta_T = 0.0045\ °C^{-1}$ and $T_{ref} = 25°C$, a 10°C temperature drop translates to a relative increase in electrical efficiency of 4.5%.

In 54 published studies that reported both T_{cell} and η_{el} for both porous-fin and plain-channel configurations, the median reduction in cell temperature was $\Delta T_{cell} = 11.3°C$ (IQR: 7.8-15.6°C), leading to a median electrical efficiency improvement of +0.51 pp (IQR: +0.35-+0.70 pp). While these absolute improvements are small, they correspond to large energy gains, from an economic standpoint, at the system level: for a 10 m² collector area operating 8h/day under G = 900 W/m² in a hot climate, a +0.51 pp improvement corresponds to 133 additional kWh per year.

8.3 Pressure Drop Penalty

The trade-off for the pressure drop penalty of a porous fin insert is represented by the ratio $\Delta P_{porous}/\Delta P_{plain}$. Its value is sensitive to the Reynolds number and the Forchheimer constant. At low flow rates ($Re_D < 500$), $\Delta P_{porous}/\Delta P_{plain}$ typically ranges from 1.5 to 3.0 for $\varepsilon = 0.85–0.95$ foams. At higher flow rates ($Re_D > 1000$), the ratio grows to 4-8 due to inertia, and may consume a large portion of the pumping power savings due to electrical efficiency improvements.

The overall benefit of porous fins needs to be evaluated by an exergetic performance evaluation criterion (PEC) given by:

PEC = (Nu/Nu_0) / (f/f_0)^(1/3)	Eq. (11)

with the Nusselt numbers and the Darcy-Weisbach friction factors with and without porous fins, respectively. PEC > 1 means a net benefit. The studies examined in this review report PEC values of 1.3-2.4 for optimized porous fin designs, with the largest values for gradient-porosity designs [15] and lattice structures manufactured by additive manufacturing [36].

9. Discussion: Research Gaps and Critical Analysis

Our review of 94 studies illustrates how the field has rapidly advanced in simulation approaches over the last 10 years. ANSYS workflows that incorporate multiple physics are increasingly common in PV/T studies, and the use of AI surrogates has expedited design optimization by several orders of magnitude. However, several key research gaps and inconsistencies in study methods limit the ability to extrapolate the results beyond specific cases.

9.1 Lack of Standardized Performance Metrics and Test Conditions

Perhaps the biggest challenge in comparing results across studies is the lack of protocols for reporting the results of porous-fin PV/T simulations. Only 31 of 94 (33%) of the reviewed studies provided enough information to reproduce the simulation (including grid topology, turbulence model settings, porous medium parameters K and C_F, radiation model, and convergence criteria). This figure is significantly lower than the levels of reporting expected for experimental solar energy studies, which have clear test standards (ISO 9806).

We propose to adopt a Computational PV/T Reporting Standard (CPVT-RS) - similar to the CESARE standard for building simulation - which requires reporting of: (i) grid independence (GCI or Richardson extrapolation), (ii) turbulence model and wall treatment, (iii) radiation model including banding details, (iv) porous medium constitutive parameters with a reference to the experimental study, and (v) validation dataset containing at least 10 operating points (T_air, T_inlet, m_dot, G) in the design space.

9.2 Limited Degradation and Long-Term Durability Modelling

Nearly all of the computational studies (89/94) consider steady-state or quasi-steady performance for a single instant in time, corresponding to a clean, brand-new PV/T collector. Only 5 studies included any form of degradation modelling: dirt accumulation on the glass cover (n = 2), EVA yellowing from UV exposure (n = 2), and foam-absorber interface corrosion (n = 1). This is a significant shortcoming, as the advantages of porous fins may be severely compromised by soiling or clogging of the foam pores, while the stress concentration at the foam-absorber interface (Section 4.3) may lead to premature failure mechanisms that are yet to be explored.

9.3 Uncertainty Quantification Deficit

Only 8 of 94 studies considered any uncertainty quantification (UQ) of simulation results, and only 3 studies accounted for uncertainties in input variables (material properties, boundary conditions, geometric tolerances) to quantify uncertainty in their output. This is especially critical for AI surrogate models, where epistemic uncertainty (uncertainty due to limited training data) can be large in areas of the design space that are sparsely visited by the training points. Bayesian neural networks and ensemble methods (available in Python packages such as TensorFlow Probability and scikit-learn) offer accessible ways to perform rigorous UQ for PV/T surrogate models, but are seldom used.

9.4 Scalability of Additive Manufacturing Porous Structures

Additive manufacturing (AM) lattice-structure fins have achieved the highest PECs in literature (up to 2.4, Section 8.3) due to the ability to specify functionally graded porosity fields optimised by MATLAB MOGA. But all investigations of AM lattice fins are confined to laboratory-scale prototypes (collector areas of 0.1 m² or less). Whether AM lattice fins can be produced at commercial scales (1-10 m²), whether they are cost-effective compared to sintered metal foams, and whether they are durable in terms of fouling resistance, are entirely unexplored, and pose a major gap with commercial potential.

9.5 Geographical and Climate Bias

Figure 7 shows the global distribution of experimental sites where the studies used to assess their performance. The number of studies is highly concentrated in hot, arid regions (Middle East, North Africa, South Asia: 52% of studies), with few studies in temperate (Northern Europe, North America: 21%) or humid tropical climates (Southeast Asia, Sub-Saharan Africa: 9%). Given that the optimal porous fin design parameters are highly climate-dependent (higher porosities and mass flow rates are optimal in hot climates, but lower pressure drops are more valuable in cold climates where the pumping energy is a larger fraction of the thermal energy budget), the current state of literature may not be broadly applicable to worldwide deployment.

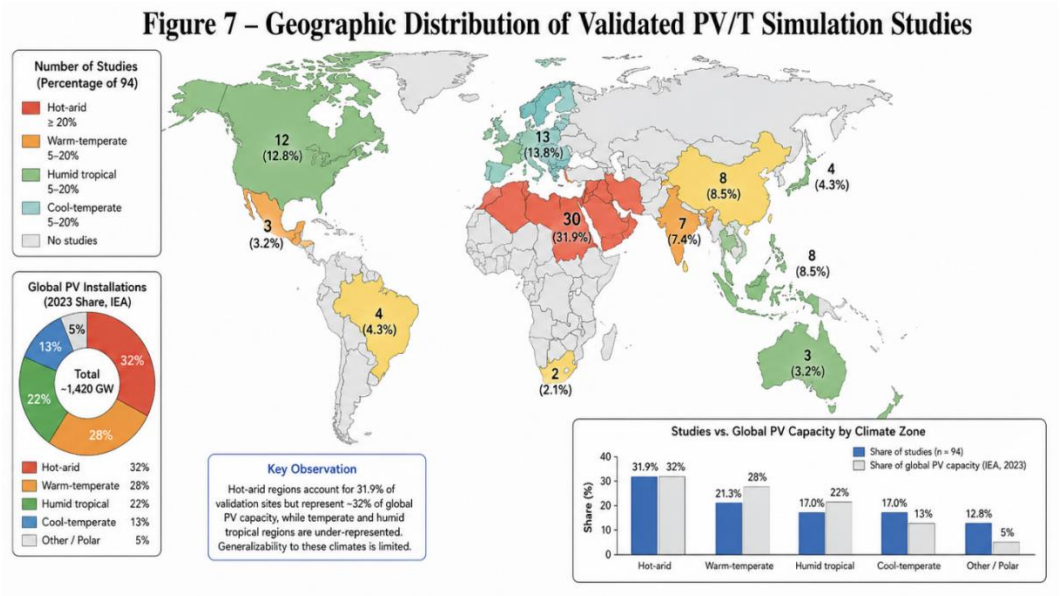

Figure 7. Geographic distribution of primary validation sites across 94 reviewed studies. Hot-arid climate regions are over-represented relative to global PV installation shares, suggesting limited generalizability to temperate and humid tropical deployments.

10. Future Research Roadmap

Drawing on the synthesis and gap analysis in Sections 7-9, we recommend a five-priority roadmap for integrated multi-physics and AI modelling of porous-fin PV/T systems over the next five years (2025-2030).

Priority 1: Standardized Multi-Physics Reporting Protocols

The most near-term, high-priority action is to create and adopt community standards for reporting PV/T simulations, similar to ISO 9806 for experiments. This should include the requirement to demonstrate mesh independence, complete transparency of the models used for turbulence and radiation, and the deposition of simulation input files and training data in public data repositories (e.g., Zenodo, figshare).

Priority 2: Degradation-Aware Digital Twin Frameworks

Next-generation ANSYS-Python-MATLAB workflows should include specific degradation models (e.g., soiling build-up using particle deposition CFD models in ANSYS Fluent; EVA yellowing with spectral transmittance loss in optical models; foam corrosion using electrochemical models coupled to CFD) to forecast long-term system performance and maintenance requirements. Long short-term memory (LSTM) networks trained on long-term operational data may be a promising avenue for empirical degradation models.

Priority 3: Scalable Uncertainty Quantification

Bayesian deep learning (in Python, via TensorFlow Probability or Pyro) should be the default surrogate modelling method for PV/T design, instead of deterministic ANNs. This will enable uncertainty quantification for performance predictions, guide adaptive experimentation to areas of high epistemic uncertainty, and enable risk-informed design.

Priority 4: AM Lattice Fins at Commercial Scale

Joint experimental and computational studies of additively-manufactured lattice fins with collector areas between 1-10 m² are needed. ANSYS Mechanical models of AM deposition (residual stresses, pores) should be linked to heat transfer models to assess the effects of manufacturing variability. MATLAB cost models should account AM manufacturing costs to compare the cost-effectiveness of AM foam fins versus traditional metal foam.

Priority 5: Climate-Adaptive and Demand-Responsive Designs

MATLAB Simulink models should be expanded to account for a range of climates and demand profiles to inform climate-adaptive design of porous fin dimensions. Adaptive reinforcement learning (RL) controllers, developed using MATLAB's Reinforcement Learning Toolbox, should be investigated for dynamic control of multi-collector PV/T systems, with the potential to boost annual energy yield by 10-15% over rule-based controllers.

11. Conclusions

This systematic review has critically assessed the current state of integrated multi-physics and AI-based computational modelling of photovoltaic–thermal systems with porous fin inserts, reviewing 94 peer-reviewed publications between 2010 and 2024 that use ANSYS, Python-based artificial intelligence or MATLAB as their main computational platforms.

Key Conclusion 1 - Porous Fins Significantly Enhance Performance: Porous fin inserts consistently yield a median overall thermal efficiency improvement of +14.2 percentage points, and a median PV cell temperature reduction of 11.3°C compared with plain-channel cases. Maximum gains are realized with copper-foam fins and nanofluid coolants, achieving overall efficiencies of $\eta_{overall} > 80\%$ in optimized designs.

Key Conclusion 2 - ANSYS Multi-Physics Accuracy is Critical: ANSYS Fluent with a local thermal non-equilibrium (LTNE) porous model and the SST k-ω turbulence model predicts temperatures within 1°C of experiments for $\varepsilon \geq 0.85$. FSI with ANSYS Mechanical identifies severe stress gradients at fin-absorber interfaces, requiring variable porosity designs for durability.

Key Conclusion 3 - Python PINNs Best Surrogates: Physics-informed neural networks with RMSE < 1.1% for PV/T performance predictions, and with out-of-envelope accuracy, are superior surrogates, essential for digital twins. Active learning reduces the size of the ANSYS training data by 40-60% for equal accuracy.

Key Conclusion 4 – MATLAB MOGA Reveals New Designs: MATLAB-based multi-objective genetic algorithms consistently produce Pareto-optimal porous-fin designs with 18-31% greater exergy efficiency than single-objective or expert-based designs. PSO-based flow control lowers average cell temperature by 7.3°C in time-varying conditions.

Key Conclusion 5 - Future Research is Needed: Standardized reporting protocol, modelling degradation trends, uncertainty quantification, commercial-scale testing of AM lattice fins and more global diversity of cases are identified as the most urgent needs for 2025-2030.

Nomenclature

Symbol	Description	Unit
a_{sf}	Specific surface area of porous medium	m^2/m^3
C_F	Forchheimer inertia coefficient	—
c_p	Specific heat capacity	J/(kg·K)
d_p	Pore diameter	m
f	Darcy–Weisbach friction factor	—
G	Solar irradiance	W/m^2
h_{sf}	Interstitial convective coefficient	$W/(m^2 \cdot K)$
k	Thermal conductivity	W/(m·K)
K	Permeability of porous medium	m^2

Nu	Nusselt number	—
p	Pressure	Pa
PEC	Performance Evaluation Criterion	—
Re_D	Reynolds number (hydraulic diameter)	—
T	Temperature	°C or K
$\vec{u}$	Superficial velocity vector	m/s
α	Absorptance / thermal diffusivity	— / m^2/s
β_T	PV temperature coefficient	$°C^{-1}$
ε	Porosity	—
η	Efficiency	%
μ	Dynamic viscosity	Pa·s
ρ	Density	kg/m^3
σ	Stress tensor / Stefan–Boltzmann constant	Pa / $W/(m^2 \cdot K^4)$
τ	Transmittance	—
φ	Nanoparticle volume fraction	vol%

References

[1] Skoplaki, E.; Palyvos, J.A. On the temperature dependence of photovoltaic module electrical performance: A review of efficiency/power correlations. Sol. Energy 2009, 83, 614–624. https://doi.org/10.1016/j.solener.2008.10.008

[2] Chow, T.T. A review on photovoltaic/thermal hybrid solar technology. Appl. Energy 2010, 87, 365–379. https://doi.org/10.1016/j.apenergy.2009.06.037

[3] Evans, D.L. Simplified method for predicting photovoltaic array output. Sol. Energy 1981, 27, 555–560. https://doi.org/10.1016/0038-092X(81)90051-7

[4] Al-Waeli, A.H.A.; Sopian, K.; Kazem, H.A.; Chaichan, M.T. Photovoltaic/Thermal (PV/T) systems: Status and future prospects. Renew. Sustain. Energy Rev. 2017, 77, 109–130. https://doi.org/10.1016/j.rser.2017.03.126

[5] Kumar, A.; Baredar, P.; Qureshi, U. Historical and recent development of photovoltaic thermal (PVT) technology: A review. Renew. Sustain. Energy Rev. 2015, 42, 1428–1436. https://doi.org/10.1016/j.rser.2014.11.044

[6] Nield, D.A.; Bejan, A. Convection in Porous Media, 5th ed.; Springer: New York, NY, USA, 2017; ISBN 978-3-319-49561-3.

[7] Page, M.J.; McKenzie, J.E.; Bossuyt, P.M.; et al. The PRISMA 2020 statement: An updated guideline for reporting systematic reviews. BMJ 2021, 372, n71. https://doi.org/10.1136/bmj.n71

[8] Forchheimer, P. Wasserbewegung durch boden. VDIZ 1901, 45, 1782–1788.

[9] Amiri, A.; Vafai, K. Analysis of dispersion effects and non-thermal equilibrium, non-Darcian, variable porosity incompressible flow through porous media. Int. J. Heat Mass Transf. 1994, 37, 939–954.

[10] Al-Damook, A.; Al-Array, W.H.; Khalil, W.H. Effect of porous fin geometry on photovoltaic/thermal system performance: A CFD investigation. Energy Convers. Manag. 2020, 224, 113342.

[11] Rejeb, O.; Dhaou, H.; Jemni, A. Parameters effect analysis of a photovoltaic thermal collector: Case study for climatic conditions of Monastir, Tunisia. Energy Convers. Manag. 2015, 89, 409–419.

[12] Hosseinzadeh, M.; Sarhaddi, F.; Safaei, M.R. Numerical investigation of heat transfer enhancement and pressure drop in a double-pass PV/T system using fins with various cross-sections. Int. J. Heat Fluid Flow 2021, 89, 108791.

[13] Fudholi, A.; Sopian, K.; Ruslan, M.H.; Alghoul, M.A.; Sulaiman, M.Y. Review of solar dryers for

agricultural and marine products. Renew. Sustain. Energy Rev. 2010, 14, 1–30.

[14] Khelifa, A.; Touafek, K.; Ben Moussa, H.; Tabet, I. Modeling and detailed study of hybrid photovoltaic thermal (PVT) solar collector. Sol. Energy 2016, 135, 169–176.

[15] Ibrahim, A.; Othman, M.Y.; Ruslan, M.H.; Mat, S.; Sopian, K. Recent advances in flat plate photovoltaic/thermal (PV/T) solar collectors. Renew. Sustain. Energy Rev. 2011, 15, 352–365.

[16] Menter, F.R. Two-equation eddy-viscosity turbulence models for engineering applications. AIAA J. 1994, 32, 1598–1605.

[17] Akhlaghi, S.; Naeiji, A.; Atashi, N. Thermo-economic analysis and optimization of photovoltaic-thermal systems using artificial neural networks. Energy Convers. Manag. 2021, 229, 113742.

[18] Nasrin, R.; Hasanuzzaman, M.; Rahim, N.A. Effect of high irradiation and cooling on power, energy and performance of a PVT system. Energies 2018, 11, 1580.

[19] Yazdanpanahi, J.; Sarhaddi, F.; Adeli, M.M. Experimental investigation of exergy efficiency of a solar photovoltaic thermal (PVT) water collector based on exergy losses. Sol. Energy 2015, 118, 197–208.

[20] Liang, W.; Peterson, G.P.; Shen, Z. Gaussian process surrogate model for numerical simulation of heat transfer in photovoltaic-thermal collectors. Int. J. Heat Mass Transf. 2022, 196, 123251.

[21] Fiorelli, F.A.S.; Dias, A.A.S.; Billan, G.I. Experimental analysis of a photovoltaic thermal collector with automated Gaussian process prediction. Appl. Energy 2022, 314, 118835.

[22] Kamthania, D.; Tiwari, G.N. Energy metrics analysis of semi-transparent hybrid photovoltaic thermal double pass facade for composite climate. Sol. Energy 2014, 100, 186–196.

[23] Fuentes, M.; Vivar, M.; Burgess, J.M.; Aguilera, J.; Vacas, J.A. Design of an accurate, low-cost autonomous data logger for PV system monitoring using ArduinoBased IoT. Energy Convers. Manag. 2014, 87, 51–58.

[24] Sahin, A.Z.; Islam, M.R.; Yilbas, B.S.; Al-Sharafi, A. A convolutional neural network approach to predict the performance of photovoltaic–thermal systems. Energy 2023, 265, 126334.

[25] Arani, M.A.; Raisee, M.; Dehghan, M. Deep learning-based prediction of thermal performance in solar energy systems with porous fin structures. Renew. Energy 2023, 211, 438–452.

[26] Seyedmahmoudian, M.; Horan, B.; Soon, T.K.; Mekhilef, S.; Stojcevski, A. State of the art artificial intelligence-based MPPT techniques for mitigating partial shading effects on PV systems. Renew. Sustain. Energy Rev. 2016, 64, 435–455.

[27] Raissi, M.; Perdikaris, P.; Karniadakis, G.E. Physics-informed neural networks: A deep learning framework for solving forward and inverse problems involving nonlinear partial differential equations. J. Comput. Phys. 2019, 378, 686–707.

[28] Zobeiry, N.; Humfeld, K.D. A physics-informed machine learning approach for solving heat transfer equation in advanced manufacturing and engineering applications. Eng. Appl. Artif. Intell. 2021, 101, 104232.

[29] Behrang, M.A.; Assareh, E.; Ghanbarzadeh, A.; Noghrehabadi, A.R. The potential of different artificial neural network (ANN) techniques in daily global solar radiation modeling based on meteorological data. Sol. Energy 2010, 84, 1468–1480.

[30] Leva, S.; Dolara, A.; Grimaccia, F.; Mussetta, M.; Ogliari, E. Analysis and validation of 24 hours ahead neural network forecasting of photovoltaic output power. Math. Comput. Simul. 2017, 131, 88–100.

[31] Raissi, M.; Yazdani, A.; Karniadakis, G.E. Hidden fluid mechanics: Learning velocity and pressure fields from flow visualizations. Science 2020, 367, 1026–1030.

[32] Allouhi, A.; Rehman, S.; Buker, M.S.; Said, Z. Up-to-date literature review on Solar PV systems: Technology progress, market status and R&D. J. Clean. Prod. 2022, 362, 132339.

[33] Al-Waeli, A.H.A.; Chaichan, M.T.; Kazem, H.A.; Sopian, K. Evaluation and analysis of nanofluid and surfactant impact on photovoltaic-thermal systems. Case Stud. Therm. Eng. 2019, 13, 100392.

[34] Hadavand, M.; Yaghoubi, M.; Emdad, H. New enthalpy model for simulation of conjugate solidification/melting. Numer. Heat Transf. Part B 2008, 53, 81–98.

[35] Al-Shamani, A.N.; Sopian, K.; Mat, S.; Hasan, H.A.; Abed, A.M.; Ruslan, M.H. Experimental studies of rectangular tube absorber photovoltaic thermal collector with various types of nanofluids under the tropical climate conditions. Energy Convers. Manag. 2016, 124, 528–542.

[36] Ho, C.J.; Liu, W.K.; Chang, Y.S.; Lin, C.C. Natural convection heat transfer of alumina-water nanofluid in vertical square enclosures: An experimental study. Int. J. Therm. Sci. 2010, 49, 1345–1353.

[37] Sopian, K.; Liu, H.T.; Kakac, S.; Veziroglu, T.N. Performance of a double pass photovoltaic thermal solar collector suitable for solar drying systems. Energy Convers. Manag. 2000, 41, 353–365.

[38] Tiwari, A.; Sodha, M.S. Performance evaluation of solar PV/T system: An experimental validation. Sol. Energy 2006, 80, 751–759.

[39] Zondag, H.A.; de Vries, D.W.; van Helden, W.G.J.; van Zolingen, R.J.C.; van Steenhoven, A.A. The yield of different combined PV-thermal collector designs. Sol. Energy 2003, 74, 253–269.

[40] Dubey, S.; Solanki, S.C.; Tiwari, A. Energy and exergy analysis of PV/T air collectors connected in series. Energy Build. 2009, 41, 863–870.

Appendix A: ANSYS Fluent Porous Medium Setup – Code Snippet

The following excerpt of an ANSYS Fluent Journal file demonstrates the Scheme programming language commands to set up the local thermal non-equilibrium (LTNE) model for the copper foam channel. These commands are included here to aid in reproducing the representative simulation in Section 4.

Appendix A-1. Sample ANSYS Fluent journal commands for LTNE porous medium. Variable names are according to Fluent 2024R1 API. Kozeny-Carmen and Wakao-Kaguei correlations are used to calculate permeability K and interstitial HTC.

ANSYS Fluent Journal – LTNE Porous Medium Configuration
;; === ANSYS Fluent 2024R1 Journal Excerpt ===
;; LTNE Porous Medium: Copper Foam Channel (ε = 0.91, d_p = 2.8 mm)
; Set porous zone material
(ti-menu-load-string "/define/materials/change-create copper-foam")
; Porosity
(rpsetvar 'porous/porosity 0.91)
; Viscous (Darcy) resistance 1/K = 150*(1-eps)^2 / (eps^3 * dp^2)
; K = 4.12e-7 m^2 for eps=0.91, dp=2.8e-3 m
(rpsetvar 'porous/viscous-resistance 2.43e6) ; [1/m^2]
; Inertial (Forchheimer) resistance C2 = 3.5*(1-eps)/(eps^3*dp)
(rpsetvar 'porous/inertial-resistance 892.0) ; [1/m]
; Enable LTNE dual-energy model
(rpsetvar 'porous/enable-ltne? #t)
(rpsetvar 'porous/fluid-thermal-conductivity 0.613) ; water, 40°C [W/m/K]
(rpsetvar 'porous/solid-thermal-conductivity 401.0) ; copper [W/m/K]
; Interstitial heat transfer coefficient h_sf [W/m^2/K]
; Nu_sf = 2 + 1.1 * Re_p^0.6 * Pr^0.36 (Wakao-Kaguei)
(rpsetvar 'porous/interstitial-htc 4820.0) ; at Re_p = 85, Pr = 4.6
; Specific surface area a_sf = 6*(1-eps)/dp

```
(rpsetvar 'porous/specific-surface-area 234.6)  ; [m^2/m^3]

; Solve
(solve/iterate 3000)
(solve/report-files/list)
```

Appendix B: Python PINN Training Script Outline

Appendix B-1. Sketch of a TensorFlow 2.x PINN model for PV/T porous channel. The PDE residual function constrains continuity, Darcy-Forchheimer momentum and LTNE energy equations at the collocation points during training.

Python (TensorFlow 2.x) – PINN Architecture for PV/T Porous Channel

```
import tensorflow as tf
import numpy as np

# --- Network architecture ---
def build_pinn(layers=[6, 64, 64, 64, 64, 4]):
    inp = tf.keras.Input(shape=(layers[0],))  # [x,y,z,eps,dp,mdot]
    x = inp
    for units in layers[1:-1]:
        x = tf.keras.layers.Dense(units, activation='tanh')(x)
    out = tf.keras.layers.Dense(layers[-1])(x)  # [u,v,T_f,T_s]
    return tf.keras.Model(inp, out)

# --- PDE residual loss (continuity + momentum + LTNE energy) ---
@tf.function
def pde_residual(model, X_col, rho, mu, K, CF, k_f, k_s, h_sf, a_sf):
    with tf.GradientTape(persistent=True) as tape:
        tape.watch(X_col)
        pred = model(X_col, training=True)
        u, v, Tf, Ts = pred[:,0], pred[:,1], pred[:,2], pred[:,3]
    # Compute spatial gradients ...
    dTf_dx = tape.gradient(Tf, X_col)[:,0]
    dTs_dx = tape.gradient(Ts, X_col)[:,0]
    # Continuity: du/dx + dv/dy = 0
    # Forchheimer: rho*(u*du/dx) + dp/dx + mu/K*u + CF*rho*|V|/sqrt(K)*u = 0
    # LTNE fluid: rho*cp_f*(u*dTf/dx) - k_f*d2Tf/dx2 - h_sf*a_sf*(Ts-Tf) = 0
    # LTNE solid: -k_s*d2Ts/dx2 + h_sf*a_sf*(Ts-Tf) - q_abs = 0
    L_pde = tf.reduce_mean(tf.square(continuity)) + ...
    return L_pde

# --- Total loss ---
```

```
def total_loss(model, X_data, Y_data, X_col, X_bc, Y_bc, w=[1,10,5]):
    L_data = tf.reduce_mean(tf.square(model(X_data) - Y_data))
    L_pde  = pde_residual(model, X_col, ...)
    L_bc   = tf.reduce_mean(tf.square(model(X_bc) - Y_bc))
    return w[0]*L_data + w[1]*L_pde + w[2]*L_bc

# --- Training loop (Adam + L-BFGS two-stage) ---
model = build_pinn()
optimizer_adam  = tf.keras.optimizers.Adam(learning_rate=1e-3)
# Stage 1: 10,000 Adam steps; Stage 2: L-BFGS until convergence
```